Facial Fracture Injury Criteria from Night Vision Goggle Impact

Martin B. Davis; Derek Y. Pang; Ian P. Herring; Cameron R. Bass

INTRODUCTION: Military personnel extensively use night vision goggles (NVGs) in contemporary scenarios. Since NVGs may induce or increase injuries from falls or vehicular accidents, biomechanical risk assessments would aid design goal or mitigation strategy development.

METHODS: This study assesses injury risks from NVG impact on cadaver heads using impactors modeled on the PVS-14 NVG. Impacts to the zygoma and maxilla were performed at 20° or 40° angles. Risks of facial fracture, neurotrauma, and neck injury were assessed. Acoustic sensors and accelerometers assessed time of fracture and provided input variables for injury risk functions. Injuries were assessed using the Abbreviated Injury Scale (AIS); injury severity was assessed using the Rhee and Donat scales. Risk functions were developed for the input variables using censored survival analyses.

RESULTS: The effects of impact angle and bone geometry on injury characteristics were determined with loading area, axial force, energy attenuation, and stress at fracture. Probabilities of facial fracture were quantified through survival analysis and injury risk functions. These risk functions determined a 50% risk of facial bone fracture at 1148 N (axial force) at a 20° maxillary impact, 588 N at a 40° maxillary impact, and 677 N at a 20° zygomatic impact. A cumulative distribution function indicates 769 N corresponds to 50% risk of fracture overall.

DISCUSSION: Results found smaller impact areas on the maxilla are correlated with higher angles of impact increasing risk of facial fracture, neck injuries are unlikely to occur before fracture or neurotrauma, and a potential trade-off mechanism between fracture and brain injury.

KEYWORDS: night vision, maxillary fracture, zygomatic fracture, orbit injury, blunt impact.

Davis MB, Pang DY, Herring IP, Bass CR. *Facial fracture injury criteria from night vision goggle impact*. Aerosp Med Hum Perform. 2023; 94(11):827–834.

Head-borne night vision goggles (NVG) have become a mainstay of modern military equipment to enhance the capabilities of both aviators and ground personnel. With NVG use increasing in militaries around the world,[5] the potential risk of NVG-induced facial trauma and eye injury from falls, vehicle and aviation crashes, and other potential impact scenarios must be evaluated. The introduction of airbag systems in military rotorcraft introduces an additional source of facial trauma through impact of the airbag on NVGs being worn.[2] This study investigates the risk of injury to facial components and provides assessments of injury severity through biomechanical analysis of NVG-equivalent indenter tests on cadaveric specimens.

While most facial impact injury studies have been conducted to improve injury assessment in automobile safety or from nonlethal projectiles, this study aims to assess the risk of facial trauma from head-mounted night vision devices, an area with limited prior work. Historically since the late 1980s, Hybrid III anthropometric test dummies initially developed for automotive crash testing were used to evaluate blunt facial impacts and specifically impacts to the zygoma and maxilla in a comparison with human cadaveric heads through the use of drop towers[1,18,26] or pneumatic impactors.[16] Further modifications of the test dummy design were examined to improve

From Duke University, Durham, NC, United States.

This manuscript was received for review in February 2023. It was accepted for publication in August 2023.

Address correspondence to: Derek Y. Pang, Associate in Research, Biomedical Engineering, Duke University Department of Biomedical Engineering, 2204 Hudson Hall Annex, Science Drive, Durham, NC 27705; derek.pang@duke.edu.

DOI: https://doi.org/10.3357/AMHP.6239.2023

biofidelity, including frangible faces.[25] Though a majority of these older facial impact studies are limited by the targeted application being automotive crash testing,[19] which would spread input forces over a larger area than the area of the ocular end of the NVG, and/or were directed at facial regions other than the orbits, studies have examined facial impact under smaller areas such as that of nonlethal ballistic impacts[21] using similar test methodologies. These studies are applicable for the establishment of a general range of force tolerance for skull constituents, which can act as an estimate for expected loads for NVG impacts. As these impacts also occur directly over the eyes and orbits, previous studies have also examined a potential for "blowout", a "hydraulic" or "buckling" fracture of the orbital floor through force transferred from intraorbital pressure of the globe or orbital rim, respectively,[22,23] on cadaveric human and living primate[11] models, which further complicates the potential mechanisms of fracture injuries under NVG impact conditions.

More recently, studies have focused on anthropomorphic tissue surrogates and modeling, testing through using porcine eyes[8] or a test series[3] on the Facial and Ocular CountermeasUre for Safety (FOCUS) head form developed by the U.S. Army.[4] Simulating eye injuries in cadaveric tissue with the rapid postmortem degradation of cadaveric eyes is a challenge.[12] A model with an ex-vivo porcine eye implanted inside a human orbit has been used to assess human ocular injuries since porcine eyes can be obtained immediately postmortem, before retinal detachments, and can be rapidly implanted.[6,12,24]

For facial injury assessment, though overall facial trauma has been characterized using the Abbreviated Injury Scale (AIS),[10] specific facial classifications, including Lefort[15] and Zingg,[27] describe detailed injury response in maxillary and zygomatic fractures, respectively. Donat[7] introduced a facial trauma classifier based on skeletal support mechanisms. More recently, Kunz[14] developed the AO Foundation's craniomaxillofacial (AOCMF) classification system for orbital fractures being either orbitozygomatic, nasoorbitoethmoidal, internal orbit, or combined orbit fractures involving the lateral (zygomatic) orbit wall, medial orbit wall, orbit floor, or orbital rim and internal components, respectively. The AOCMF system describes the first three fracture types as isolated, despite the possibility of overlapping, and introduces "blowout" as the injury mechanism of these three classifications in causing fracture via release of intraorbital pressure.

Global concussive head injury may be assessed with the Head Impact Criterion (HIC) for concussive head injury[20] based on the Wayne State Concussive Tolerance Curve.[17] HIC is defined as:

$$HIC = \left\{ (t_2 - t_1) \left[\frac{1}{t_2 - t_1} \int_{t_1}^{t_2} a(t)\,dt \right]^{2.5} \right\}_{\max}$$

where t_1 and t_2 are the initial and final times (in seconds) of the interval during which HIC attains a maximum value; therefore, HIC includes the effect of head acceleration and duration. When the acceleration is expressed in g, an HIC value of 1000 is specified as the level for onset of severe head injury. The maximum time duration of HIC is limited to a specific value, usually 15 ms. Physically, HIC predicts that large accelerations may be tolerated for short times. HIC may be evaluated using the triaxial accelerometer at the head center of gravity.

The three principal goals of this study were to: 1) characterize NVG impact injuries to the eye and other regions using a novel method of instrumenting cadaver models, 2) elucidate loading tolerances of different regions of the orbit structure, and 3) develop region-specific quantitative risk assessments of orbital injuries from NVG impact through statistical survival analysis. NVG impact injuries were also examined in the context of the proposed and existing facial injury criteria.

METHODS

Subjects

Cadaveric testing oversight was provided by the University of Virginia Cadaver Use Committee. Physical parameters from the sectioned specimens used in this series are summarized in **Table I**. Mean specimen total body mass was 73 ± 21 kg and

Table I. Specimen Demographics and Anthropometry Summary.

	SPECIMEN							
GENERAL INFORMATION	**FRM-105**	**FRF-125**	**FRM-130**	**FF-131**	**FF-132**	**FRM-151**	**FRM-109**	**FRF-137**
Demographic								
Gender	M	F	M	F	F	M	M	F
Age at death	57	59	93	84	80	63	69	75
Mass (kg)	119	68	49	59	68	68	76	76
Stature (cm)	177.0	167.6	167.6	162.6	165.1	167.6	175.3	167.5
Anthropometry								
Head circ (cm)	56.0	54.2	54.6	53.6	53.0	61.1	53.6	52.9
Head breadth (cm)	15.0	13.5	14.4	14.0	14.0	15.0	13.5	14.2
Head depth (cm)	19.7	20.5	23.5	19.5	18.0	20.5	21.0	17.7
Head height (cm)	24.3	21.3	20.0	21.5	21.5	24.5	22.5	18.0
Head + neck mass (kg)	6.59	5.39	5.44	4.26	4.44	6.91	5.90	5.39
Potting level	T3	T4	C4	C3	C4	T4	C7	T1
Pot to O/C2 (cm)	15.0	17.2	3.5	2.0	4.5	16.0	6.0	6.5

mean stature was 169 ± 5 cm. Mean age at death was 72.5 ± 13 yr. The mean mass and stature are comparable to the 50th percentile man (70 kg, 176.8 cm). Pretest CT imaging was performed to ensure no pretest injuries.

Equipment

A pneumatic impactor and a transfer piston provided the impact. The 6.5-kg transfer piston was mounted on a low-friction mount to provide "free flight" conditions for the mass, typical of impact head/helmet mass, while limiting overall impactor stroke. High-frequency impact components were reduced using a foam decelerator mounted on the transfer piston. The impactor was calibrated to produce a piston velocity of $16\,ft \cdot s^{-1}$ ($5\,m \cdot s^{-1}$) measured by high-speed video analysis. This velocity is representative of a fall from 4.17 ft (1.27 m; i.e., less than average head height) and the input energy was ~81 J. This initial kinetic energy can be transmitted to the specimen in several ways: as strain energy in the soft and hard tissues, including fracture formation, or as kinetic energy of the specimen.

A triaxial load cell (PCB 260A, PCB Piezoelectronics, Depew, NY, United States) mounted between a simulated NVG end (US PVS-14 machined in aluminum) and the traveling mass was the primary impact assessment in axial force and shear. The positioning fixture (**Fig. 1**) used a pair of pneumatic pistons to provide adjustment in the z direction (superior–inferior). A linear bearing track, mounted across the top of two pistons, provided free motion in the x direction (anterior-posterior). A second bearing at a 90° angle to the x-axis provided free motion in the y direction (medial–lateral). An adjustable index was mounted to the lower track with x-y-z-axis rotation adjustments. A six-axis load cell (IF-210, First Technology Safety Systems, Novi, MI, United States) connected the neck potting cup to the index. All tests were recorded at 1000 frames per second using high-speed digital video. One camera (Phantom V, Vision Research, Wayne, NJ, United States) was positioned at the side of the fixture at the height of the specimen. A second camera (Kodak RO, Kodak, Rochester, NY, United States) was positioned above the fixture.

To determine the time of fracture, a pair of acoustic sensors (Nano/Pico, Physical Acoustics, Princeton Junction, NJ, United States) were glued using cyanoacrylate adhesive bilaterally to the skull. To provide a comparison with existing injury criteria, an array of accelerometers (Endevco 7270A-2K, Endevco, San Juan Capistrano, CA, United States) was mounted in the upper mandible. An additional accelerometer (Endevco 7270A-2K) was mounted on the transfer piston to measure impact mass deceleration. The instrumentation is shown in Fig. 1. Sensor output was recorded and converted to digital data by a custom high-speed data acquisition system. The data collection process was controlled with LabView software. The sample rate was 1 MHz for all channels and 64 ms of data were recorded.

Procedure

For impact, the Frankfort Plane of the specimen was aligned parallel to the local horizontal with the midsagittal plane of the specimen aligned with the x-axis. The index was adjusted about the z-axis to position the specimen for a zygoma impact or adjusted in the x-z plane for a maxilla impact. 20° and 40° impacts to the maxilla and zygoma were chosen as a reasonable range given the use case of the night vision goggle application. The fixture was then adjusted along the x-axis (anterior–posterior axis) so that the NVG profile would contact the specimen at the point in space where the transfer piston began free flight. Due to postmortem degradation of the cadaver globes and to more accurately simulate normal anatomy, the human cadaver globes were enucleated and replaced with fresh porcine globes, which were affixed by attachment of cadaver rectus muscles to the porcine globe sclera. Immediately before the test, the porcine eye was pressurized to physiological conditions by injecting the anterior chamber with saline followed by stromal hydration to prevent fluid egress. After the first test on each specimen, the untested side was palpated to ensure that fractures did not transfer from the tested side.

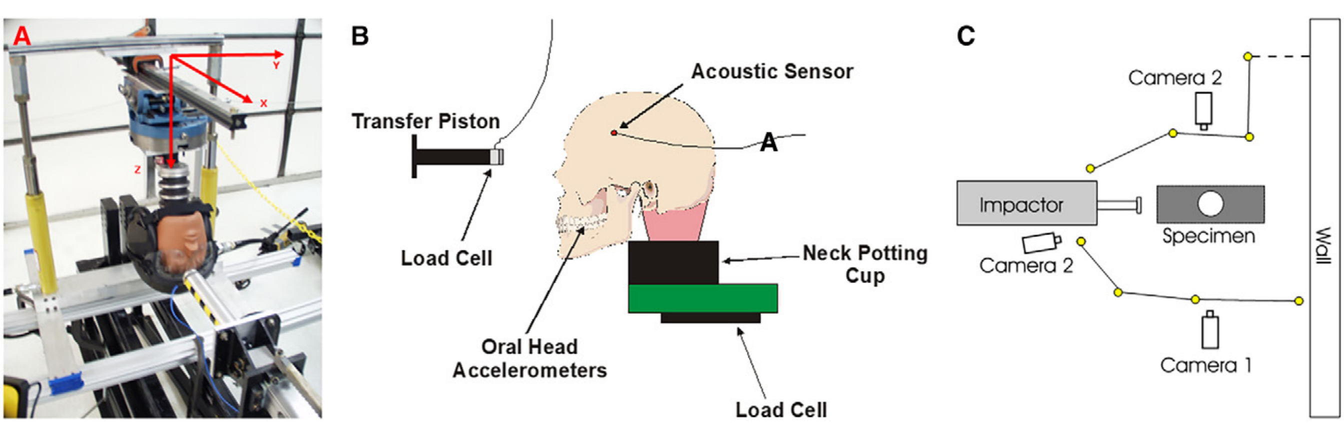

Fig. 1. A) The positioning fixture, transfer piston, and axes with placeholder Hybrid III head. B) Instrumentation overview including fixture/piston locations and specimen orientation. C) Overhead diagram of test environment.

Force/deflection characteristics were calculated using load cell data and video displacement data. Energy transferred to the specimen during the impact was calculated using video analysis. The position in space of the impacting device was determined for each video frame over the course of the event. A parametric force-deflection plot was then created using the displacement and force time histories. Then work done was found by integrating this force-displacement curve. The energy to fracture onset and the energy to the end of fracture (both as measured by the acoustic signal) were measured for the tests. The kinetic energy of the specimen was determined by integrating the acceleration signals from the nine-axis array to produce corresponding velocity time histories.

The peak velocity and specimen mass were used to find the peak kinetic energy of the specimen. To examine the impact of strain energy relative to specimen kinetic energy or fracture formation, an estimated value can be calculated with a few assumptions. For a linear elastic material, the strain energy per unit volume is given by:

$$W = \frac{\sigma\varepsilon}{2}$$

where σ represents the stress and ε represents the strain. Using Hooke's Law (σ = Eε) and multiplying by the contact area and thickness yields an equation for strain energy:

$$E_{strain} = \frac{E\varepsilon^2 At}{2}$$

where *E* is the elastic modulus, *A* is the area, and *t* is the skin thickness. Relative areas of impact can be ascertained by dividing energy (work done) by the force at the time of acoustic onset and squaring the result to provide a scaling measurement in terms of area that can be used to compare the different loading conditions.

To assess injury severity for zygoma impact, each of the fracture patterns was graded according to the scales used by Rhee[18] and Donat[7] The Rhee scale has the advantage of being specific to facial fracture, allowing finer distinctions to be made between similar injuries. For the Donat system, the number of buttress and beam segments that have been compromised by fracture were counted to produce a whole number score.[7]

Statistical Analysis

For this study, injury timing is assessed as the onset of fracture indicated by acoustic emission. The axial force at fracture is used as the input to the statistical models. A survival analysis based on a logistic distribution was performed on the dataset of force at acoustic onset for these tests.[13] The cumulative distribution function for the logistic distribution assumes a form of:

$$1 - \frac{1}{1 + e^{\frac{(A-F)}{B}}}$$

where F is the force in Newtons, A is the mean, and B is the "Scale" parameter. For this distribution, the mean of the dataset corresponds to a 50% risk of injury. Minitab 15 (Minitab, LLC, State College, PA, United States) was used to determine the parameter values for the data set.

RESULTS

The test matrix with impact conditions and injury assessments is shown in **Table II**. All tests except for Test 1.1 resulted in some fracture. There were few eye injuries produced in this test series; those that did occur were minor (AIS 1). Corneal abrasions resulted in Tests 1.2, 1.10, and 1.12; minor folding or shifting of the sclera occurred in Test 1.6. Representative axial force time histories for each test type are shown in **Fig. 2**.

Average peak axial force and axial force at initial fracture are shown in Fig. 2. Statistically significant differences (*t*-test, a = 0.05) were found for initial fracture force between the 20° and 40° zygoma impacts, and between the 40° zygoma and the 40° maxilla impacts.

All Nij values for neck injury were below the injury tolerance of 1.0 (**Table III**). To assess the influence of facial impact on neck injury level, a one-way ANOVA was performed using the Nij neck injury criterion for angle of impact and impact location with respective *P*-values of 0.12 and 0.05 (**Fig. 3**). This statistically significant difference in neck injury criterion between zygomatic and maxillary impacts suggests maxillary impacts are more likely to increase the risk of neck injury.

To assess head injury, calculated HIC values for the tests are shown in **Table IV**. One of the tests, NVG 1.1, resulted in a HIC value greater than 1000, indicative of potentially injurious skull/brain trauma. This test had a substantial portion of the input energy and momentum transferred to the head (68 J of kinetic energy from 81 J of input energy) but saw no fracture. The remainder of the HIC values seen in the testing were in the range of ~50–300, suggesting the risk of concussive injury from

Table II. Test Instrumentation.

MEASUREMENT	SENSOR LOCATION	AXIS	SENSOR TYPE	MANUFACTURER	MODEL
Impact force	NVG eyepiece	X, Y, Z	3-axis load cell	PCB	260A
Impactor acceleration	Transfer piston	Axial	Uniaxial accelerometer	Endevco	7270A-2K
Head acceleration	Cadaver mouth (9)	X, Y, Z	Nine axis array	Endevco	7270A-6K
Fracture detection	Left/right parietal skull (2)	N/A	Ultrasonic	Physical acoustics	Nano/Pico
Neck load, moment	Neck potting cup	X, Y, Z	6-axis load cell	First technology safety systems	IF-210

NVG: night vision goggles.

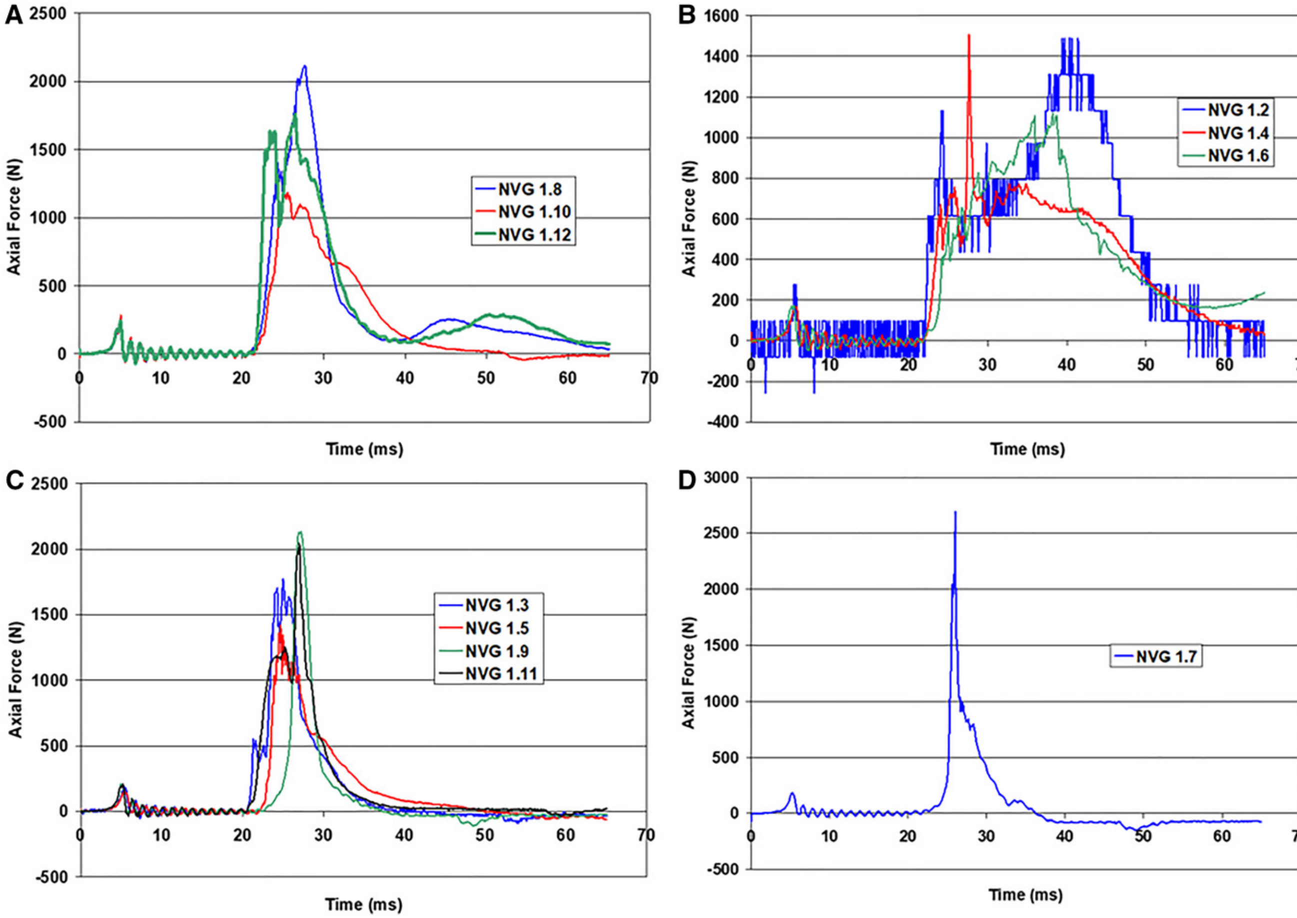

Fig. 2. Axial force time histories for: A) 20° maxilla impacts; B) 40° maxilla impacts; C) 20° zygoma impacts; and D) 40° zygoma impacts.

these impacts is low and that unmodified HIC is not a good indicator of facial fracture.

Survival analysis injury risk functions were calculated for the 20° and 40° maxilla impact scenarios and the 20° zygoma impacts (**Fig. 4**). A force of 1148 N corresponds to a 50% risk of fracture for the 20° maxilla case, 588 N for the 40° maxilla case, and 677 N for the 20° zygoma case. For the cumulative distribution function for overall survival in all impact scenarios, a force of 769 N corresponds to a 50% risk of fracture. These results with 95% confidence intervals are shown in Fig. 4.

DISCUSSION

Several parameters play key roles in characterizing injury type/severity and assessing risk due to NVG impact injuries. Of particular interest is the role facial fracture plays in reducing energy

Table III. Summary of Injury Severity.

	ORBIT INJURY SEVERITY			EYE INJURY SEVERITY					
TEST	AIS	RHEE	DONAT	INJURY	AIS	IMPACT SIDE	IMPACT LOCATION	IMPACT ANGLE	ACOUSTIC EMISSION Δt
1	0	1	0			R	zygoma	40°	12.7
2	3	6	6	corneal abrasion	1	L	maxilla	40°	23.8
3	3	5	4			R	zygoma	20°	13.2
4	3	6	5			L	maxilla	40°	13.3
5	3	6	5			R	zygoma	20°	7.9
6	3	6	6	sclera fold	1	L	maxilla	40°	18.5
7	2	2	1			R	zygoma	40°	3.5
8	3	3	3			L	maxilla	20°	5.5
9	2	2	0			R	zygoma	20°	11.1
10	3	6	6	corneal abrasion	1	L	maxilla	20°	9.5
11	3	2	1			R	zygoma	20°	11.3
12	3	5	2	corneal abrasion	1	L	maxilla	20°	9.1

AIS: Abbreviated Injury Scale; RHEE: Rhee scale—Rhee et al.[18]; DONAT: Donat et al.[7]

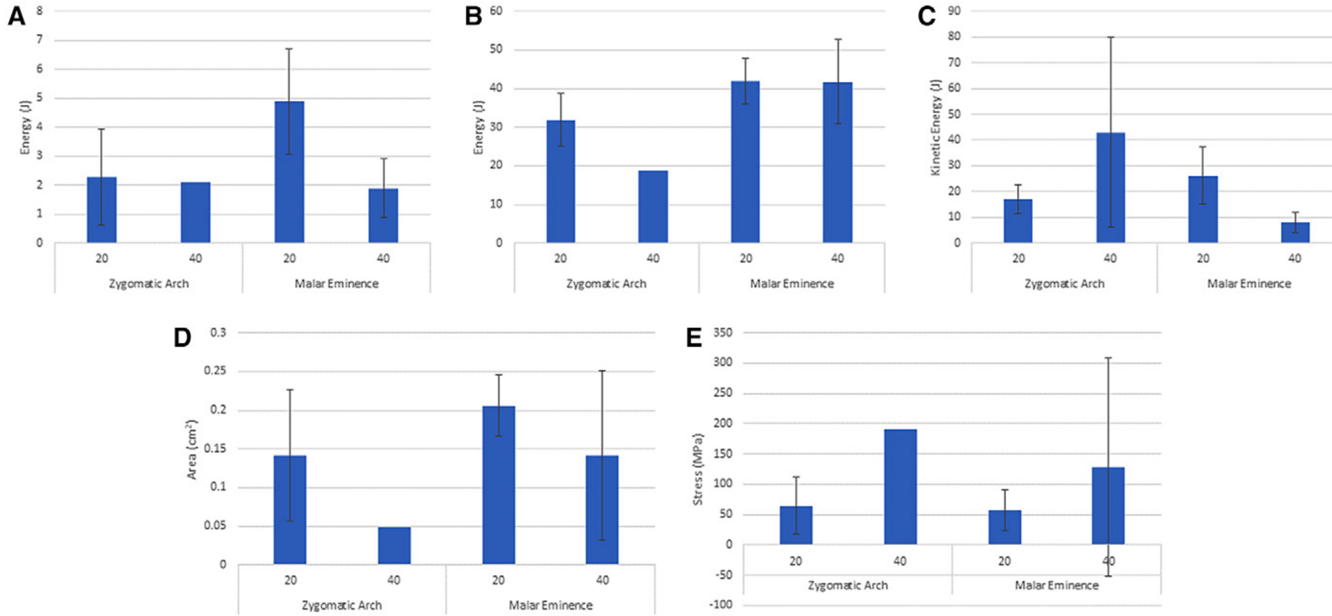

Fig. 3. Energy (± 1 SD) to: A) fracture initiation; B) end of fracture; C) peak specimen kinetic energy (± 1 SD) for the NVG series; D) area (± 1 SD) for the loading conditions; and E) stress (± 1 SD) at fracture.

transfer to further impact or injure the brain. During the one test in which facial fracture did not occur (Test 1.1), a larger fraction of the input energy was transferred to the rigid body motion of the head, producing an HIC value associated with head injury. This suggests there is a tradeoff between facial fracture and brain trauma, and that the occurrence of facial fracture may limit the risk of brain trauma. All other cases produced some degree of facial fracture with less energy transfer to rigid body motion, emphasizing the tradeoff between facial fracture and the potential of blunt neurotrauma from facial impact.

To estimate the effect of the viscoelastic properties of skin on the energy/force to fracture, Gadd[9] performed drop tests on facial skin samples at similar rates to these tests, with an elastic modulus of ~3.2 MPa with a peak strain of 0.7. Assuming a mean skin thickness of the specimens in this test series of 5 mm with NVG contact area of ~1/6 of the NVG profile area (230 mm^2), the energy storage in the skin is less than 1 J at peak strain. So, the skin energy storage is small compared with the overall input energy to the system (~79 J). Thus, the bulk of the input energy is spent either creating fractures or applying bulk kinetic energy in the specimen.

For injury severity, significant differences were found with respect to injury location and impact angle, largely from geometric effects of the underlying facial bones. Impacts to the zygoma tend to be less severe than impacts to the maxilla because the zygomatic impact is more tangential to the lateral side of the face while the maxillary impact is more normal to the front of the face. Between the 20° and 40° zygoma impacts, the 40° condition is less injurious because the NVG contacts the strong frontal bone before it reaches the zygoma. The 20° maxilla impact is generally less severe than the 40° impact because the facial bones support the more direct blow better than they do the higher angle blow,

Table IV. Summary of Measured Parameters: Axial Forces, Energy, Injury Criteria.

				AXIAL FORCES (N)			ENERGY (J)				
TEST	SPECIMEN	LOCATION	ANGLE	PEAK	ACOUSTIC ONSET	Nij	TO FRACTURE	AT PEAK FORCE	PEAK RES ACC (g)	HIC	HIC DURATION (ms)
1	FF-132	zygoma	40						223	1009	2.6
7	FRM-151	zygoma	40	2692	946	0.2	6.11	10.75	125	128	2.7
3	FRM-130	zygoma	20	1772	501	0.33	4.98	17.39	105	134	3.2
5	FF-131	zygoma	20	1421	968	0.31	7.47	10.22	85	102	5.8
9	FRF-125	zygoma	20	2133	166	0.22	4.3	14.21	104	210	3.2
11	FRM-105	zygoma	20	2015	997	0.31	9.76	32.55	138	179	6
2	FF-132	maxilla	40	1569	695	0.75			115	105	5.6
4	FRM-130	maxilla	40	1506	619	0.39	7.54	19.41	106	59	8.6
6	FF-131	maxilla	40	1119	414	0.72	6.24	39.04	82	147	15
8	FRM-151	maxilla	20	2104	1250	0.42	11.06	30.28	87	233	8.8
10	FRF-125	maxilla	20	1179	578	0.19	8.08	15.92	47	73	8.6
12	FRM-105	maxilla	20	1760	1495	0.51	10.65	26.7	166	299	5.4

HIC: Head Impact Criterion.

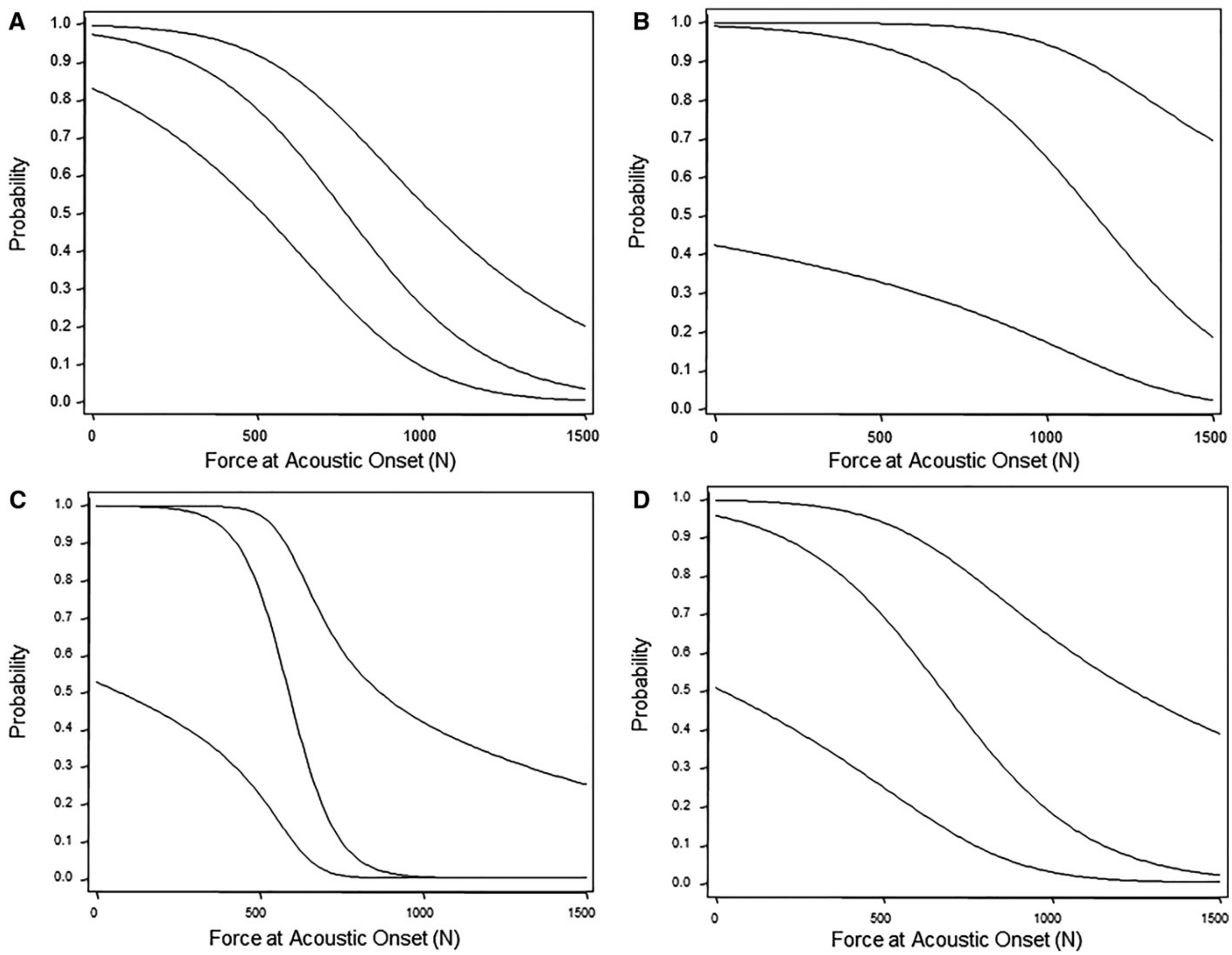

Fig. 4. Logistic survival plots for: A) all tests (50% fracture at 769 N); B) 20° maxilla case (50% fracture at 1148 N); C) 40° maxilla case (50% fracture at 588 N); and D) 20° zygoma case (50% fracture at 677 N).

which includes some shearing load. The impacts that were better supported, such as the 20° maxilla impact, require a higher energy input before the bones begin to fracture.

The survival analysis risk functions for impact peak force in this study here are consistent with previous literature.[18] Rhee found that axial forces for the zygomatic impacts range from 1359–4565 N where the current study range is 1421–2692 N with a more tightly constrained geometry. However, the peak axial force does not accurately relate to fracture tolerance of the facial bone. In addition, this study provides accurate characterization of fracture tolerances using fracture initiation identified with acoustic sensors. This use of incipient fracture formation force rather than peak force produces a realistic and accurate metric of fracture risk.

There are several important limitations in this study. Results from the porcine eye replacements showed little risk of injury to the globe beyond superficial corneal abrasions. There was little damage to the eyes from orbital floor blowout, despite the frequency of that type of injury. Since porcine eyes are generally slightly smaller than human eyes and postmortem shrinkage of orbital contents likely occurs, the model may have limited the potential for globe rupture or orbital blowout injury and resultant tissue impingement. Information about the start of crack formation provided by the acoustic sensors indicates that injury may occur at levels that are well below the peak tolerance.

In conclusion, this study used a combined cadaver-porcine head model to assess injuries to the eye and facial bones for NVG facial impact injuries. Several key factors were found to affect injury risk, including impact location, angle, axial force, and energy attenuation. Of significance are the contexts for the different injury mechanisms: facial fracture is more likely to occur with increased angle of impact at the maxilla (Fig. 4), with correspondingly lower energies for fracture initiation (Fig. 3A) owing to geometric factors, including bony support. For the zygoma, the tangential angle and influence of the frontal bone affects the injury risk. Blunt impact brain injury from NVG impact is more likely for cases without fracture, since facial fracture crack formation attenuates input energy; the nonfracture scenario transferred more kinetic energy to the head with an injurious HIC value (1009). Neck injury is impact location dependent (Table IV), but is altogether unlikely to occur before facial fracture or brain injury (all tests below the injury reference value of 1).

In this study, the tolerance of the facial bones to NVG impacts in different locations, directions, and conditions was assessed using acoustic sensors to detect the time of crack formation and injury parameters such as energy, axial force, and stress at fracture initiation. The risk of bony fracture was quantified at each impact location and for all facial fractures as a function of force with the use of statistical survival analysis. Finally, the severity of the injuries seen for the various loading conditions was assessed.

This work suggests several areas for future research. NVG-indenter testing on different models may help evaluate model fidelity, and testing models possessing midface region arrays of load cells such as the FOCUS head form may facilitate force distribution mapping. Advancements in night vision technology such as adoption of panoramic (GPNVG) or thermal fusion modules have also resulted in differences in overall NVG weights and dimensions and would necessitate further evaluation for a wider variety of impact scenarios.

ACKNOWLEDGEMENTS

Financial Disclosure Statement: The authors have no competing interests to declare.

Authors and Affiliations: Martin B. Davis, BSE, MS, Cold Spring Harbor Laboratory, Cold Spring Harbor, NY, United States; Derek Y. Pang, BSE, MS, Duke Injury Biomechanics Laboratory, Duke University, Durham, NC, United States; Ian P. Herring, DVM, MS, VA-MD College of Veterinary Medicine, Virginia Tech, Blacksburg, VA, United States; and Cameron R. “Dale” Bass, BS, Ph.D., Department of Bioengineering, Wayne State University, Detroit, MI, United States.

REFERENCES

1. Allsop DL, Warner CY, Wille MG, Schneider DC, Nahum AM. Facial impact response—a comparison of the Hybrid III dummy and human cadaver. SAE Trans. 1988; 97(Section 4):1224–1240.
2. Bass C, Davis M, Stitzel J, Duma S. Airbag interaction with night vision goggles. Report to the United States Army Aeromedical Research Laboratory. Ft. Rucker (AL): U.S. Army Aeromedical Research Laboratory; 2002.
3. Bir C, Sherman D, MacDonald R, Esquivel A. Assessment of less lethal impact munitions using the Facial and Ocular CountermeasUre for Safety (FOCUS) headform. Hum Factors Mech Eng Def Saf. 2022; 6:2.
4. Bisplinghoff J, Cormier J, Duma S, Kennedy E, Depinet P, Brozoski F. Development and validation of eye injury and facial fracture criteria for the focus headform. Blacksburg (VA): Virginia Polytechnic Institute and State University; 2008.
5. Chrzanowski K. Review of night vision technology. Opto-Electron Rev. 2013; 21(2):153–181.
6. Dave K. Development of a porcine and human eye finite element model to investigate ocular injury thresholds in impact and blast loading conditions [Thesis]. Detroit (MI): Wayne State University; 2019.
7. Donat TL, Endress C, Mathog RH. Facial fracture classification according to skeletal support mechanisms. Arch Otolaryngol Head Neck Surg. 1998; 124(12):1306–1314.
8. Duma SM, Bisplinghoff JA, Senge DM, McNally C, Alphonse VD. Evaluating the risk of eye injuries: intraocular pressure during high speed projectile impacts. Curr Eye Res. 2012; 37(1):43–49.
9. Gadd CW, Nahum AM, Schneider DC, Madeira RG. Tolerance and properties of superficial soft tissues in situ. SAE Technical Paper 700910, 14th Stapp Car Crash Conference. Warrendale (PA): SAE; 1970.
10. Gennarelli TA, Wodzin E. AIS 2005: a contemporary injury scale. Injury. 2006; 37(12):1083–1091.
11. Green RP Jr, Peters DR, Shore JW, Fanton JW, Davis H. Force necessary to fracture the orbital floor. Ophthal Plast Reconstr Surg. 1990; 6(3): 211–217.
12. Kennedy EA, Ng TP, McNally C, Stitzel JD, Duma SM. Risk functions for human and porcine eye rupture based on projectile characteristics of blunt objects. Stapp Car Crash J. 2006; 50:651–671.
13. Kent RW, Funk JR. Data censoring and parametric distribution assignment in the development of injury risk functions from biochemical data. SAE Technical Paper 2004-01-0317; SAE 2004 World Congress & Exhibition. Warrendale (PA): SAE; 2004.
14. Kunz C, Audigé L, Cornelius C-P, Buitrago-Téllez CH, Rudderman R, Prein J. The comprehensive AOCMF classification system: orbital fractures-level 3 tutorial. Craniomaxillofac Trauma Reconstr. 2014; 7(1, Suppl.):92–102.
15. Le Fort R. Etude experimentale sur les fractures de la machoire superieure. Revue Chirurgio. 1901; 23:208–227.
16. Nyquist GW, Cavanaugh JM, Goldberg SJ, King AI. Facial impact tolerance and response. SAE Trans. 1986; 95(Section 5):850–871.
17. Patrick LM, Lissner HR, Gurdjian ES, editors. Survival by design: head protection. Proceedings of the American Association for Automotive Medicine Annual Conference; 1963. Chicago (IL): Association for the Advancement of Automotive Medicine; 1963.
18. Rhee JS, Posey L, Yoganadan N, Pintar F. Experimental trauma to the malar eminence: fracture biomechanics and injury patterns. Otolaryngol Head Neck Surg. 2001; 125(4):351–355.
19. Schneider DC, Nauhm AM, editors. Impact studies of facial bones and skull. Proceedings: Stapp Car Crash Conference. Warrendale (PA): Society of Automotive Engineers; 1972.
20. Versace J. A review of the Severity Index. Proceedings: Stapp Car Crash Conference. Warrendale (PA): Society of Automotive Engineers; 1971.
21. Viano DC, Bir C, Walilko T, Sherman D. Ballistic impact to the forehead, zygoma, and mandible: comparison of human and frangible dummy face biomechanics. J Trauma Acute Care Surg. 2004; 56(6): 1305–1311.
22. Warwar RE, Bullock JD, Ballal DR, Ballal RD. Mechanisms of orbital floor fractures: a clinical, experimental, and theoretical study. Ophthal Plast Reconstr Surg. 2000; 16(3):188–200.
23. Waterhouse N, Lyne J, Urdang M, Garey L. An investigation into the mechanism of orbital blowout fractures. Br J Plast Surg. 1999; 52(8):607–612.
24. Watson RA. Comparative computational models of the human and porcine eye [Dissertation]. San Antonio (TX): The University of Texas at San Antonio; 2020.
25. Welbourne E, Ramet M, Zarebski M, editors. A comparison of human facial fracture tolerance with the performance of a surrogate test device. Proceedings of the 12th International Technical Conference on Experimental Safety Vehicles; May 29-June 1, 1989; Göteborg, Sweden. [Accessed 1 Sept. 2023]. Available from https://wbldb.lievers.net/10125898.html.
26. Yoganandan N, Pintar F, Sanees A Jr, Harris G, Chintapalli K, et al. Steering wheel induced facial trauma. SAE Trans. 1988; 97(Section 4): 1104–1128.
27. Zingg M, Laedrach K, Chen J, Chowdhury K, Vuillemin T, et al. Classification and treatment of zygomatic fractures: a review of 1,025 cases. J Oral Maxillofac Surg. 1992; 50(8):778–790.